Articles

Modulation of Tryptophan Environment in Membrane-Bound Melittin by Negatively Charged Phospholipids: Implications in Membrane Organization and Function[†]

Anindya K. Ghosh, R. Rukmini, and Amitabha Chattopadhyay*

Centre for Cellular and Molecular Biology, Uppal Road, Hyderabad 500 007, India

Received August 5, 1997; Revised Manuscript Received September 15, 1997[⊗]

ABSTRACT: Melittin is a cationic hemolytic peptide isolated from the European honey bee, *Apis mellifera*. Since the association of the peptide in the membrane is linked with its physiological effects, a detailed understanding of the interaction of melittin with membranes is crucial. We have investigated the interaction of melittin with membranes of varying surface charge in the context of recent studies which show that the presence of negatively charged lipids in the membrane inhibits membrane lysis by melittin. The sole tryptophan residue in melittin has previously been shown to be critical for its hemolytic activity. The organization and dynamics of the tryptophan residue thus become important to understand the peptide activity in membranes of different charge types. Wavelength-selective fluorescence was utilized to monitor the tryptophan environment of membrane-bound melittin. Melittin exhibits a red edge excitation shift (REES) of 5 nm when bound to zwitterionic membranes while in negatively charged membranes, the magnitude of REES is reduced to 2−3 nm. Further, wavelength dependence of fluorescence polarization and near-UV circular dichroism spectra reveal characteristic differences in the tryptophan environment for melittin bound to zwitterionic and anionic membranes. These studies are supported by time-resolved fluorescence measurements of membrane-bound melittin. Tryptophan penetration depths for melittin bound to zwitterionic and anionic membranes were analyzed by the parallax method [Chattopadhyay, A., and London, E. (1987) *Biochemistry 26*, 39−45] utilizing differential fluorescence quenching obtained with phospholipids spin-labeled at two different depths. Our results provide further insight into molecular details of membrane lysis by melittin and the modulation of lytic activity by negatively charged lipids.

Melittin, the principle toxic component in the venom of the European honey bee, *Apis mellifera*, is a small linear peptide (NH$_2$-GIGAVLKVLTTGLPALISWIKRKRQQ-CONH$_2$) composed of 26 amino acids and is known to have a powerful hemolytic activity (*1*, *2*). It is a cationic peptide with a large hydrophobic region (residues 1−20) and a stretch of predominantly hydrophilic amino acids (residues 21−26) at the carboxy-terminal end of the molecule which give rise to its amphiphilic character. This amphiphilic property of melittin makes it water soluble and yet it spontaneously associates with natural and artificial membranes (for reviews, see refs 3−7). Such a sequence of amino acids, together with the amphiphilic nature, is characteristic of many membrane-bound peptides and putative transmembrane helices of membrane proteins (*4*, *5*, *8*). This has resulted in melittin being used as a simple model to study lipid−protein interactions in membranes (*3−7*). In addition to its strong hemolytic activty, melittin induces voltage-dependent ion

channels across planer lipid bilayers and causes bilayer micellization and membrane fusion (*3−5*, *9*).

The conformation of melittin is known to be largely random coil when present as free monomer in solution (*5*, *10*). However, it self associates to form an α-helical tetrameric structure driven by the formation of a hydrophobic core at high ionic strength, pH, or melittin concentration (*5*, *10*). The peptide adopts an α-helical conformation when bound to membranes or micelles (*5*, *11−13*). The X-ray crystal structure of the aqueous tetramer is known with high (2 Å) resolution (*14*), although the structure of the membrane-bound form is not known. Interaction of melittin with membranes has attracted considerable attention since the association of the peptide in the membrane is linked with its physiological effects (*4*, *5*). These studies assume broader significance from the fact that the amphiphilic α-helical conformation of this cytolytic toxin in membranes resembles those of apolipoproteins and peptide hormones (*15−17*), signal peptides (*11*, *18*, *19*), the envelope glycoprotein gp41 from the human immunodeficiency virus (HIV) (*20*, *21*), the pore-forming peptide of pathogenic *Entamoeba histolytica* (*22*, *23*), and the 25-residue presequence (p25) for subunit IV of yeast cytochrome oxidase (*24*). The state of aggregation of melittin when bound to membranes (*25−28*), its depth of penetration into the membrane (*29−31*), its orientation

---

* Address correspondence to this author. Telephone: +91-40-7172241. Fax: +91-40-7171195. E-mail: amit@ccmb.ap.nic.in.

relative to the plane of the bilayer (*13*, *32*), and the dependence of its membrane interaction on factors such as the physical state of the membrane as well as the length of the fatty acyl chains (*33*) have been the subjects of considerable research. In spite of the number of studies, however, there appears to be no consensus regarding the orientation, depth of penetration into the membrane, or aggregation state of membrane-bound melittin (*5*).

Melittin has a single fluorescent residue, Trp-19, and has no other aromatic amino acid residue. This makes the tryptophan a sensitive probe to study the interaction of melittin with membranes (*29*−*31*, *33*−*38*). The importance of the sole tryptophan residue of melittin in its hemolytic activity has been demonstrated by the remarkable decrease in activity observed upon photooxidation of the tryptophan (*39*) and upon substitution of Trp-19 by leucine (*40*). This is further supported by studies with individual amino acid omission analogues of melittin (*41*) and the introduction of a second tryptophan residue in melittin sequence (*42*). These studies point out the crucial role played by the uniquely positioned tryptophan in maintaining the structure (*43*, *44*) and hemolytic activity (*41*, *42*) of membrane-bound melittin. In addition, fluorescence quenching and molecular modelling studies point out the involvement of Trp-19 in the interaction of melittin with its specific inhibitors (*45*). The organization and dynamics of the immediate environment around the tryptophan thus become important for the activity of the peptide. We have previously monitored the microenvironment experienced by the sole tryptophan in melittin bound to membranes composed of zwitterionic lipids (DOPC)[1] utilizing wavelength-selective fluorescence approach (*36*). Our results indicated that the tryptophan residue is located in a motionally restricted region in the membrane which may have important functional consequences.

Wavelength-selective fluorescence comprises a set of approaches based on the red edge effect in fluorescence spectroscopy which can be used to directly monitor the environment and dynamics around a fluorophore in a complex biological system (*46*). A shift in the wavelength of maximum fluorescence emission toward higher wavelengths, caused by a shift in the excitation wavelength toward the red edge of absorption band, is termed the red edge excitation shift (REES). This effect is mostly observed with polar fluorophores in motionally restricted media such as very viscous solutions or condensed phases (*46*−*49*). This phenomenon arises from the slow rates of solvent relaxation (reorientation) around an excited state fluorophore, which is a function of the motional restriction imposed on the solvent molecules in the immediate vicinity of the fluorophore. By utilizing this approach, it becomes possible to probe the mobility parameters of the environment itself (which is represented by the relaxing solvent molecules) using the fluorophore merely as a reporter group. Further, since the ubiquitous solvent for biological systems is water, the information obtained in such cases will come from the otherwise "optically silent" water molecules although the involvement of polar moieties such as lipid carbonyl groups cannot be ruled out. This makes REES and related techniques extremely useful in biology since hydration plays a crucial modulatory role in a large number of important cellular events (*50*), including lipid−protein interactions (*51*) and ion transport (*52*−*54*). We have previously shown that REES and related techniques (wavelength-selective fluorescence approach) serve as a powerful tool to monitor organization and dynamics of probes and peptides bound to membranes or micelles (*55*−*61*).

Melittin is known to interact selectively with negatively charged lipids (*5*, *34*, *62*−*64*). The affinity of melittin for membranes composed of negatively charged lipids has been shown to be about 100-fold greater than for zwitterionic lipids (*65*). Melittin is also known to modulate lipid organization in membranes depending on the nature of the lipid component (*31*, *66*−*68*). The functional significance of interaction of melittin with negatively charged lipids is brought out by recent studies (*69*−*71*) which show that the presence of negatively charged lipids in the membrane inhibits the lytic power of melittin and that the inhibition is enhanced with increasing surface charge density.

In this paper, we report the effects of red edge excitation on the fluorescence characteristics of the sole tryptophan in melittin, when bound to membranes containing anionic lipids (DOPG and DOPA), and the zwitterionic lipid DOPC. We have previously shown from wavelength-selective fluorescence studies that the tryptophan in melittin, when bound to membranes composed of DOPC, is located in a motionally restricted region of the membrane (*36*). Since biological membranes in general, and red blood cell membranes (the site of hemolytic action of melittin) in particular, contain negatively charged lipids (often distributed asymmetrically among the two leaflets), the selective interaction of melittin with these lipids assume physiological significance. In this paper, we have thus extended wavelength-selective fluorescence studies to membranes composed of negatively charged lipids. In addition, to gain a better understanding of the molecular details of melittin−membrane interaction, we have determined the precise membrane penetration depths of the tryptophan residue in case of zwitterionic and negatively charged membranes. This was done by utilizing the parallax method (*72*), which involved quenching of the fluorescence of the sole tryptophan by spin-labeled phospholipids, where the spin-label (nitroxide group) was attached to various positions of the fatty acyl chain. Our results indicate an interfacial localization of the melittin tryptophan in its membrane-bound form. This is consistent with the general finding that tryptophan residues in membrane proteins and peptides are predominantly localized in the membrane interface (*57*, *60*; also see Results). Further, we have analyzed the environment and organization of the membrane-bound tryptophan as well as the peptide backbone by circular dichroism spectroscopy.

These results show that wavelength-selective fluorescence, when used in combination with membrane depth analysis, promises to be a powerful tool to monitor lipid−protein

---

[1] Abbreviations: 2-AS, 2-(9-anthroyloxy)stearic acid; 12-AS, 12-(9-anthroyloxy)stearic acid; CD, circular dichroism; CF, carboxyfluorescein; DMPC, dimyristoyl-*sn*-glycero-3-phosphocholine; DOPA, dioleoyl-*sn*-glycero-3-phosphatidic acid; DOPC, dioleoyl-*sn*-glycero-3-phosphocholine; DOPG, dioleoyl-*sn*-glycero-3-phosphatidylglycerol; EDTA, ethylenediaminetetraacetic acid; ESR, electron spin resonance; MARCKS, myristoylated alanine-rich protein *C* kinase substrate; MLV, multilamellar vesicle; MOPS, 3-(*N*-morpholino)propanesulfonic acid; NBD, 7-nitrobenz-2-oxa-1,3-diazol-4-yl; NBD-PE, *N*-(7-nitrobenz-2-oxa-1,3-diazol-4-yl)-1,2-dipalmitoyl-*sn*-glycero-3-phosphoethanolamine; 5-PC, 1-palmitoyl-2-(5-doxyl)stearoyl-*sn*-glycero-3-phosphocholine; 12-PC, 1-palmitoyl-2-(12-doxyl)stearoyl-*sn*-glycero-3-phosphocholine; REES, red edge excitation shift; SUV, small unilamellar vesicle; TLC, thin-layer chromatography.

interactions, especially involving electrostatic component as in melittin−membrane interaction. Furthermore, we show that careful analysis of fluorescence polarization as a function of emission wavelength brings out important differences in the microenvironment experienced by the tryptophan of melittin bound to membranes of different charge types. Near-UV CD spectra of the membrane-bound peptide in these two cases also bring out such differences. Our results provide a mechanistic framework for the differential lytic activity of the peptide in membranes with different surface charges.

EXPERIMENTAL PROCEDURES

Materials. Melittin of the highest available purity, DMPC, and carboxyfluorescein were obtained from Sigma Chemical Co. (St. Louis, MO). DOPC, DOPG, DOPA, and the spin-labeled phospholipids (5- and 12 PC) were purchased from Avanti Polar Lipids (Birmingham, AL). The 2- and 12-AS were from Molecular Probes (Eugene, OR). Lipids were checked for purity by TLC on silica gel precoated plates (Sigma) in chloroform/methanol/water (65:35:5, v/v/v) and were found to give only one spot in all cases with a phosphate-sensitive spray and on subsequent charring (*73*). The concentrations of the phospholipids were determined by phosphate assay subsequent to total digestion by perchloric acid (*74*). DMPC was used as a standard to assess lipid digestion. The concentration of melittin in aqueous solution was calculated from its molar extinction coefficient of 5570 M^{-1} cm^{-1} at 280 nm (*75*). To check for phospholipase A_2 contamination in melittin, phospholipase activity was assayed using ^{14}C-labeled DOPC obtained from Amersham International (*76*). All other chemicals used were of the highest purity available. Solvents used were of spectroscopic grade. Water was purified through a Millipore (Bedford, MA) Milli-Q system and used throughout.

Assay of Actual Spin Content in Spin-Labeled Lipids by Fluorescence Quenching. The actual spin (nitroxide) content of the spin-labeled phospholipids was assayed (*77*) using fluorescence quenching of anthroyloxy-labeled fatty acids (2- and 12-AS) by determining the percent of uncalibrated spin-labeled phospholipid that had to be incorporated into MLVs of DOPC to give the same quenching as an ESR-calibrated sample with 15% spin-labeled phospholipid (*78*). For this, samples were made with a total lipid concentration of 125 μM (*78*). MLVs were prepared containing 5 (or 12)-PC and DOPC (a total of 160 nmol of these two lipids as per phosphate assay done prior to this) and 1.37 nmol of 2 (or 12)-AS by drying the lipid mixture under a stream of nitrogen and then under a high vacuum for at least 3 h, followed by addition of 1.28 mL buffer (10 mM acetate, 150 mM NaCl, pH 5.0) and vigorous vortexing for 2 min. This particular pH was chosen to avoid ground state heterogeneity of AS probes due to carboxyl ionization state (*79*). The final concentration of the fluorophore (2- or 12-AS) was 1.07 μM giving rise to a lipid/fluorophore ratio of 117:1 (mol/mol). Triplicates were made for each sample. Fluorescence intensity was measured with an excitation wavelength of 365 nm and an emission wavelength of 461 nm. Excitation and emission slits corresponding to band-pass of 5 and 10 nm, respectively, were used. Fluorescence intensity was obtained from the average of two 5 s readings. Samples were kept in the dark for 30 s between two readings and stirred with a magnetic stirrer. Background samples

without AS probes gave negligible fluorescence (much less than 1%) and were subtracted from the sample fluorescence. The ratio of spins per molecule was found to be 0.74 and 0.76 for 5-PC and 12-PC, respectively.

Sample Preparations. Three types of small unilamellar vesicles (SUVs) were made each containing 2% (mol/mol) melittin and having the following lipid compositions: (a) DOPC, (b) 40% DOPC/60% DOPG (mol/mol), and (c) 50% DOPC/50% DOPA (mol/mol). These vesicles were prepared by drying 640 nmol (2560 nmol for CD measurements) of total lipid (DOPC, DOPC/DOPG, or DOPC/DOPA in the above proportions) under a stream of nitrogen while being warmed gently (35 °C) and then under a high vacuum for at least 3 h. The lipids were swollen by adding 1.5 mL of 10 mM MOPS, 150 mM NaCl, pH 7.0 buffer containing 5 mM EDTA, and vortexed for 3 min to disperse the lipid. The lipid dispersions were then sonicated until they were clear (7−20 min, in bursts of 2 min, while being cooled in ice) using a Branson model 250 sonifier fitted with a microtip. The sonicated samples were centrifuged at 15 000 rpm for 20 min to remove any titanium particle shed from the microtip during sonication. To incorporate melittin into membranes, a small aliquot containing 12.8 nmol (51.2 nmol for CD measurements) of melittin was added from a stock solution in water to the preformed vesicles and mixed well. Samples were kept in the dark for 12 h before measuring fluorescence. Background samples were prepared in the same way except that melittin was not added to them. All experiments were done at room temperature (25 °C).

For depth measurements using the parallax method, liposomes were made by the ethanol injection method (*80, 81*). These samples were made by drying 640 nmol of total lipid (DOPC or DOPC/DOPG) containing 15 mol% spin-labeled phospholipid (5- or 12-PC) under a stream of nitrogen while being warmed gently (35 °C) and then under a high vacuum for at least 3 h. The dried lipids were then dissolved in ethanol to give a final concentration of 40 mM. The ethanolic lipid solution was then injected into 10 mM MOPS, 150 mM NaCl, pH 7.0 buffer containing 5 mM EDTA, while vortexing to give a final concentration of 0.43 mM total lipid in the buffer. Melittin was incorporated into membranes by adding a small aliquot containing 12.8 nmol of melittin from a stock solution in water to the pre-formed vesicles and mixed well to give membranes containing 2% melittin. In terms of phospholipids, these samples contained either DOPC (85%) and 5 (or 12)-PC (15%) or DOPC (25%), 5 (or 12)-PC (15%), and DOPG (60%). Duplicate samples were prepared in each case except for samples lacking the quencher (5- or 12-PC) for which triplicates were prepared. Background samples lacking the fluorophore (melittin) were prepared in all experiments, and their fluorescence intensity was subtracted from the respective sample fluorescence intensity. Samples were kept in the dark for 12 h before measuring fluorescence.

Steady State Fluorescence Measurements. Steady state fluorescence measurements were performed with a Hitachi F-4010 spectrofluorometer using 1 cm path length quartz cuvettes. Excitation and emission slits with a nominal band-pass of 5 nm were used for all measurements. All spectra were recorded using the correct spectrum mode. Background intensities of samples in which melittin was omitted were subtracted from each sample spectrum to cancel out any contribution due to the solvent Raman peak and other

scattering artifacts. Fluorescence polarization measurements were performed using a Hitachi polarization accessory. Polarization values were calculated from eq 1 (*82*):

$$P = \frac{I_{VV} - GI_{VH}}{I_{VV} + GI_{VH}} \qquad (1)$$

where I_{VV} and I_{VH} are the measured fluorescence intensities with the excitation polarizer vertically oriented and emission polarizer vertically and horizontally oriented, respectively. G is the grating correction factor and is equal to I_{HV}/I_{HH}. All experiments were done with multiple sets of samples and average values of polarization are shown in the figures. The spectral shifts obtained with different sets of samples were identical in most cases. In other cases, the values were within ±1 nm of the ones reported.

For depth measurements, samples were excited at 280 nm and emission was collected at 334 nm. Excitation and emission slits with a nominal band-pass of 5 nm were used. Fluorescence was measured at room temperature and averaged over two 5-second readings. Intensities were found to be stable over time. In all cases, the intensity from background samples without fluorophore was subtracted. Membrane penetration depths were calculated using eq 5 (see Results).

Time-Resolved Fluorescence Measurements. Fluorescence lifetimes were calculated from time-resolved fluorescence intensity decays using a Photon Technology International (London, Western Ontario, Canada) LS-100 luminescence spectrophotometer in the time-correlated single photon counting mode. This machine uses a thyratron-gated nanosecond flash lamp filled with nitrogen as the plasma gas (16 ± 1 in. of mercury vacuum) and is run at 22−25 kHz. Lamp profiles were measured at the excitation wavelength using Ludox as the scatterer. To optimize the signal to noise ratio, 5000 photon counts were collected in the peak channel. All experiments were performed using slits with a nominal band-pass of 4 nm or less. The sample and the scatterer were alternated after every 10% acquisition to ensure compensation for shape and timing drifts occurring during the period of data collection. The data stored in a multichannel analyzer was routinely transferred to an IBM PC for analysis. Intensity decay curves so obtained were fitted as a sum of exponential terms:

$$F(t) = \sum \alpha_i \exp(-t/\tau_i) \qquad (2)$$

where α_i is a pre-exponential factor representing the fractional contribution to the time-resolved decay of the component with a lifetime τ_i. The decay parameters were recovered using a nonlinear least squares iterative fitting procedure based on the Marquardt algorithm (*83*). The program also includes statistical and plotting subroutine packages (*84*). The goodness of the fit of a given set of observed data and the chosen function was evaluated by the reduced χ^2 ratio, the weighted residuals (*85*), and the autocorrelation function of the weighted residuals (*86*). A fit was considered acceptable when plots of the weighted residuals and the autocorrelation function showed random deviation about zero with a minimum χ^2 value (generally not more than 1.5). Mean (average) lifetimes $<\tau>$ for biexponential decays of fluorescence were calculated from the decay times and pre-exponential factors using the following equation (*87*):

$$<\tau> = \frac{\alpha_1\tau_1^2 + \alpha_2\tau_2^2}{\alpha_1\tau_1 + \alpha_2\tau_2} \qquad (3)$$

Global Analysis of Lifetimes. The primary goal of the nonlinear least-squares (discrete) analysis of fluorescence intensity decays discussed above is to obtain an accurate and unbiased representation of a single fluorescence decay curve in terms of a set of parameters (*i.e.*, α_i, τ_i). However, this method of analysis does not take advantage of the intrinsic relations that may exist between the individual decay curves obtained under different conditions. A condition in this context refers to temperature, pressure, solvent composition, ionic strength, pH, excitation/emission wavelength, or any other independent variable which can be experimentally manipulated. This advantage can be derived if multiple fluorescence decay curves, acquired under different conditions, are simultaneously analyzed. This is known as the global analysis in which the simultaneous analyses of multiple decay curves are carried out in terms of internally consistent sets of fitting parameters (*88−91*). Global analysis thus turns out to be very useful for the prediction of the manner in which the parameters recovered from a set of separate fluorescence decays vary as a function of an independent variable, and helps distinguish between models proposed to describe a system.

In this paper, we have obtained fluorescence decays as a function of excitation and emission wavelengths. The global analysis, in this case, assumes that the lifetimes are linked among the data files (*i.e.*, the lifetimes for any given component are the same for all decays), but that the corresponding pre-exponentials are free to vary. This is accomplished by using a matrix mapping of the fitting parameters in which the pre-exponentials are unique for each decay curve while the lifetimes are mapped out to the same value for each decay. All data files are simultaneously analyzed by the least squares data analysis method using the Marquardt algorithm (as described above) utilizing the map to substitute parameters appropriately while minimizing the global χ^2. The normalized global χ^2 values obtained were in the range of 1.1−1.7. The software used for the global analysis was obtained from Photon Technology International (London, Western Ontario, Canada).

Circular Dichroism (CD) Measurements. CD measurements were carried out at room temperature (25 °C) on a JASCO J-715 spectropolarimeter which was calibrated with (+)-10-camphorsulfonic acid (*92*). The spectra were scanned in a quartz optical cell with a path length of 0.1 cm (for far-UV spectra) or 1 cm (for near-UV spectra). All spectra were recorded in 0.2 nm wavelength increments with a 4 s response and a band width of 1 nm. For monitoring changes in secondary structure, spectra were scanned in the far-UV range from 205 to 250 nm at a scan rate of 50 nm/min. Each spectrum is the average of 5 scans with a full scale sensitivity of 50 mdeg. Tertiary structural changes were followed by scanning the spectra in the near-UV range from 260 to 315 nm at a scan rate of 100 nm/min. In this case, the full scale sensitivity was set at 5 mdeg and each spectrum is the average of 20 scans. All spectra were corrected for background by subtraction of appropriate blanks and were smoothed making sure that the overall shape of the spectrum
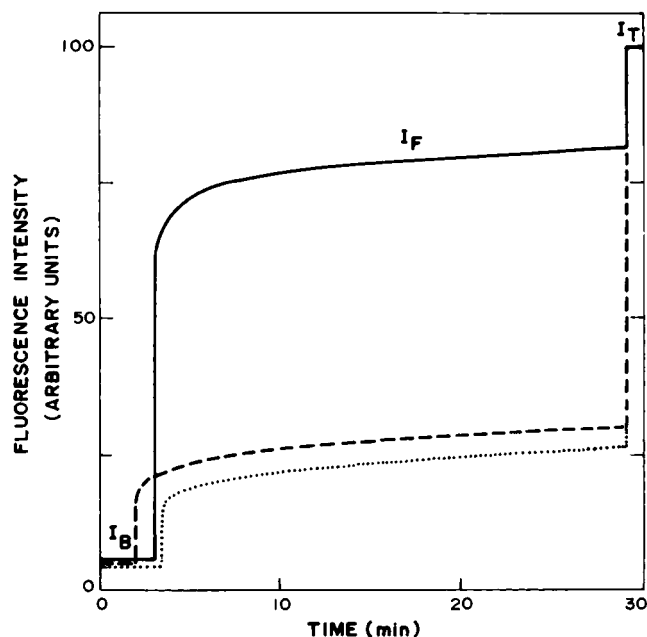
FIGURE 1: Release of entrapped CF induced by melittin in vesicles of DOPC (—), DOPC/DOPG (···), and DOPC/DOPA (- - -). I_B is the background (self-quenched) intensity of CF encapsulated in vesicles, while I_F represents the enhanced fluorescence intensity resulting from dilution of the dye in the medium caused by melittin induced release of entrapped CF. I_T is the total fluorescence intensity after complete permeabilization is achieved upon addition of Triton X-100. Lipid concentration was 0.43 mM, and melittin to lipid ratio was 1:50 (mol/mol). See Experimental Procedures for other details.

remains unaltered. Data are represented as molar ellipticities and were calculated using the formula

$$[\theta] = \theta_{obs}/(10Cl) \tag{4}$$

where θ_{obs} is the observed ellipticity in mdeg, l is the path length in cm, and C is the melittin concentration in mol/L. The concentration of melittin used for the CD measurements was 34.17 μM.

Permeabilization of Lipid Vesicles. The ability of melittin to cause release of entrapped vesicle contents for zwitterionic (DOPC) and negatively charged (40% DOPC/60% DOPG or 50% DOPC/50% DOPA) vesicles was checked by monitoring the increase in fluorescence intensity of carboxyfluorescein (CF), encapsulated in vesicles at high self-quench concentrations, upon addition of melittin (*93*). Lipids in organic solvents were first dried under a stream of nitrogen followed by high vacuum. Lipid films thus obtained were dispersed in a buffer containing 10 mM MOPS, 75 mM NaCl, and 50 mM CF (pH 7.4) and sonicated in a Branson model 250 sonifier. Liposomes were separated from non-encapsulated (free) CF by gel filtration on a Sephadex G-75 column using an elution buffer of 10 mM MOPS, 150 mM NaCl and 5 mM EDTA (pH 7.4), and lipid concentrations were estimated by complexation with ammonium ferrothiocyanate (*94*). Fluorescence was measured at room temparature (25 °C) with a Hitachi F-4010 spectrofluorometer using 1 cm path length quartz cuvettes. The excitation wavelength was 490 nm and emission was set at 520 nm. Excitation and emission slits with a nominal band-pass of 3 nm were used. The high concentration (50 mM) of the entrapped CF led to self-quenching of its fluorescence resulting in low fluorescence intensity of the vesicles (I_B, see Figure 1). An

aliquot of melittin solution in water was then added and mixed properly to obtain the desired peptide to lipid ratio. Release of CF caused by addition of melittin led to the dilution of the dye into the medium and could therefore be monitored by an enhancement of fluorescence intensity (I_F). This enhancement of fluorescence is a measure of the extent of vesicle permeabilization. Fluorescence was continuously monitored after the addition of melittin to the vesicles. The experiments were normalized relative to the total fluorescence intensity (I_T) corresponding to the complete release of CF after complete disruption of all the vesicles by addition of Triton X-100 (2% v/v). CF release could not be detected with vesicles alone (without any addition of melittin) in the time scale of the experiment.

RESULTS

Since bee venom contains an endogenous phospholipase A_2 (*5*), the purity of melittin used was checked by phospholipase assay on vesicle samples containing radiolabeled phospholipids (*76*). Although no phospholipase A_2 activity could be detected for shorter incubations, some activity was found upon prolonged incubation. This activity was found to be totally inhibited by the addition of 5 mM EDTA. Experiments were thus performed using buffers containing 5 mM EDTA in order to avoid any possible artifacts caused by phospholipase contamination (*5*). After completion of the fluorescence experiments, lipids were checked for degradation by TLC on silica gel plates as described above (see Experimental Procedures). Even after keeping the samples for a few days at room temperature, no lysoPC could be detected.

Melittin-Induced Leakage of Vesicle Contents: Effect of Vesicle Charge

The effect of negatively charged lipids on the lytic power of melittin is shown in Figure 1. This figure shows the release of CF entrapped in vesicles composed of DOPC, or DOPC mixed with either DOPG or DOPA, induced by melittin. Initially, a low background fluorescence (I_B) is observed in all cases since the high concentration (50 mM) of CF used resulted in self-quenching of fluorescence. Upon addition of melittin, the entrapped CF was released into the buffer due to lysis induced by melittin. This led to the dilution of the dye which gave rise to increased fluorescence (I_F). The extent of increase in fluorescence intensity is a measure of the lytic power of melittin in a given membrane environment. Relative lytic efficiencies were determined by complete disruption of the vesicle membranes with Triton X-100 which corresponded to the total fluorescence (F_T). As is evident from the figure, the lytic efficiency of melittin in different vesicles is clearly dependent on the composition of the membrane. Thus, while there is about 80% lysis in DOPC vesicles, it is reduced to 25−30% in vesicles containing DOPG or DOPA at the same lipid/peptide ratio (see Figure 1). This is in agreement with previous studies in which it was shown that the presence of negatively charged lipids inhibits membrane lysis induced by melittin (*69−71*).

Fluorescence of Membrane-Bound Melittin

The fluorescence emission maximum of melittin in different environments is shown in Table 1. The emission maximum undergoes a blue shift of 17−20 nm when
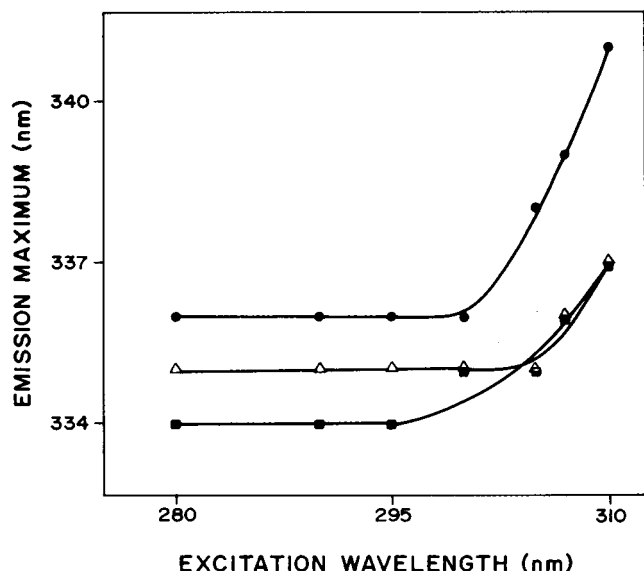
FIGURE 2: Effect of changing excitation wavelength on the wavelength of maximum emission for melittin in vesicles of DOPC (●), DOPC/DOPG (■), and DOPC/DOPA (△). Melittin to lipid ratio was 1:50 (mol/mol). See Experimental Procedures for other details.

Table 1: Fluorescence Emission Characteristics of Melittin in Different Environments

medium	composition	emission maximum[a] (nm)	REES (nm)
membrane			
zwitterionic	DOPC	336	5
anionic	DOPC/DOPG	334	3
anionic	DOPC/DOPA	335	2
buffer[b]	10 mM MOPS	353	—
	150 mM NaCl		
	5 mM EDTA, pH 7.0		

[a] Excitation wavelength 280 nm. [b] The concentration of melittin in buffer was 8.53 μM. All other conditions are as in Figure 2.

incorporated into membranes due to a decrease in polarity of the surrounding matrix. The emission maximum of melittin incorporated into DOPC vesicles is around 336 nm, as has been reported previously (*36*). There is a further blue shift of 1−2 nm when melittin is bound to negatively charged vesicles containing DOPG or DOPA, in agreement with previous reports (*31, 34, 67*).

Red Edge Excitation Shift of Membrane-Bound Melittin

The shifts in the maxima of fluorescence emission[2] of the tryptophan residue of melittin in vesicles composed of DOPC, DOPC/DOPG, and DOPC/DOPA as a function of excitation wavelength are shown in Figure 2. As the excitation wavelength is changed from 280 to 310 nm, the emission maxima are shifted from 336 to 341 nm in case of vesicles containing only DOPC, from 334 to 337 nm for DOPC/DOPG vesicles, and from 335 to 337 nm for vesicles containing DOPC/DOPA. These correspond to REES of 5 nm for DOPC vesicles and to REES of 3 and 2 nm for vesicles containing DOPG and DOPA, respectively (see Table 1). It is possible that there could be further red shift when melittin is excited beyond 310 nm. We found it difficult to work in this wavelength range because of very low signal to noise ratio and artifacts due to the Raman peak that remained even after background subtraction. Such shifts in the wavelength of emission maxima with change in the excitation wavelength are characteristic of the red edge effect and indicate that the tryptophan is localized in a motionally restricted environment in these cases. Since the average location of the tryptophan residue in membrane-bound melittin is at the membrane interface (see Results), such a

result would directly imply that this region of the membrane offers considerable restriction to the reorientational motion of the solvent dipoles around the excited state tryptophan. This is in agreement with our previous observations that the NBD group of NBD-PE, which is located at a similar position in DOPC bilayer (*72, 95*), and the interfacial tryptophans of the membrane-bound gramicidin channel, also experience a similar restriction to mobility from the surrounding membrane environment (*56, 57*). The interfacial region of the membrane is characterized by unique motional (*96−99*) and dielectric (*100*) properties different from the bulk aqueous phase and the more isotropic hydrocarbon-like deeper regions of the membrane (*46*). This specific region of the membrane is also known to participate in intermolecular charge interactions (*101*) and hydrogen bonding through the polar head group (*102, 103*). These structural features which slow down the rate of solvent reorientation have been recognized as typical environmental features which give rise to appreciable red edge effects (*104*).

The most striking feature of the above results is that the magnitude of REES is different for melittin bound to membranes composed of lipids of different head group charges. Thus, while a REES of 5 nm is observed in membranes made of zwitterionic lipids (DOPC), the corresponding value in membranes containing anionic lipids (DOPG or DOPA) is 2−3 nm, depending on the lipid type. This observation is significant since it shows that wavelength-selective fluorescence in general, and REES in particular, is sensitive to lipid−protein interactions involving electrostatic forces. Since electrostatic interactions play a very crucial role in lipid−protein interactions in many cases (see Discussion), this should offer a novel way to monitor such interactions.

Polarization Changes with Excitation Wavelength

In addition to the shift in emission maximum on red edge excitation, fluorescence polarization is also known to be dependent on excitation wavelength in motionally restricted media (*46* and references therein). The excitation polarization spectra (*i.e.*, a plot of steady state polarization *vs* excitation wavelength) of melittin in different model membranes and in buffer, are shown in Figure 3. The polarization of melittin in buffer remains essentially invariant over the range of excitation wavelengths. On the other hand, polarizations in membranes change upon altering the excitation wavelength, with a sharp increase toward the red edge of the absorption band. Such an increase in polarization upon red edge excitation for peptides and proteins containing tryptophans as well as other aromatic fluorophores, especially

---

[2] We have used the term "maximum of fluorescence emission" in a somewhat wider sense here. In every case, we have monitored the wavelength corresponding to maximum fluorescence intensity, as well as the center of mass of the fluorescence emission. In most cases, both these methods yielded the same wavelength. In cases where minor discrepancies were found, the center of mass of emission has been reported as the fluorescence maximum.
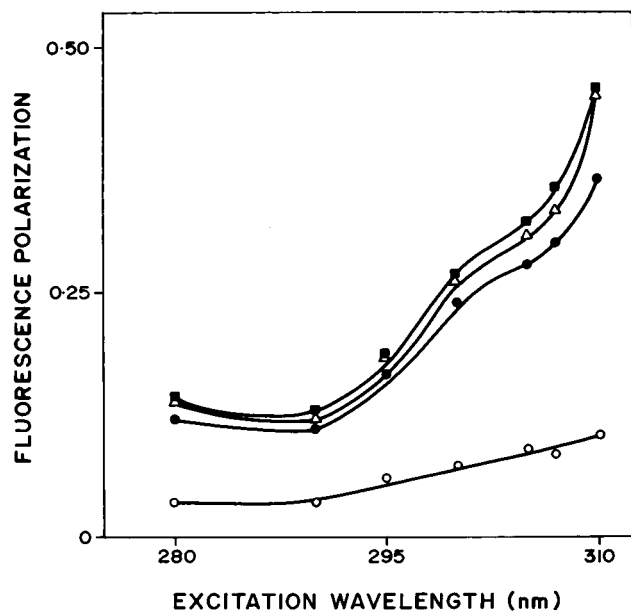
FIGURE 3: Fluorescence polarization of melittin as a function of excitation wavelength in buffer (○) and vesicles of DOPC (●), DOPC/DOPG (■), and DOPC/DOPA (△). Polarization values were recorded at 334 nm. Melittin to lipid ratio was 1:50 (mol/mol) in different vesicles. The concentration of melittin in buffer was 8.53 μM. See Experimental Procedures for other details.

Table 2: Lifetimes of Membrane-Bound Melittin as Functions of Excitation Wavelength[a]

excitation wavelength (nm)	α_1	τ_1 (ns)	α_2	τ_2 (ns)
(a) DOPC				
294	0.91 (0.91)[b]	0.54 (0.54)	0.09 (0.09)	3.86 (3.93)
296	0.95 (0.91)	0.29 (0.54)	0.05 (0.09)	3.62 (3.93)
305	0.94 (0.95)	0.51 (0.54)	0.06 (0.05)	3.42 (3.93)
313	0.96 (0.98)	0.54 (0.54)	0.04 (0.02)	2.79 (3.93)
316	0.96 (0.98)	0.52 (0.54)	0.04 (0.02)	2.66 (3.93)
(b) DOPC/DOPG				
294	0.88 (0.90)	0.60 (0.54)	0.12 (0.10)	3.36 (3.40)
296	0.89 (0.91)	0.54 (0.54)	0.11 (0.09)	3.11 (3.40)
305	0.85 (0.92)	0.45 (0.54)	0.15 (0.08)	2.50 (3.40)
313	0.97 (0.98)	0.51 (0.54)	0.03 (0.02)	2.60 (3.40)
316	0.96 (0.98)	0.54 (0.54)	0.04 (0.02)	2.70 (3.40)
(c) DOPC/DOPA				
294	0.91 (0.91)	0.54 (0.54)	0.09 (0.09)	3.42 (3.42)
296	0.90 (0.91)	0.60 (0.54)	0.10 (0.09)	3.30 (3.42)
305	0.90 (0.94)	0.40 (0.54)	0.10 (0.06)	2.45 (3.42)
313	0.95 (0.98)	0.52 (0.54)	0.05 (0.02)	2.42 (3.42)
316	0.94 (0.98)	0.54 (0.54)	0.06 (0.02)	2.29 (3.42)

[a] Emission wavelength 350 nm. [b] Numbers in parentheses are the results of global analysis.

in media of reduced mobility has been reported before (*56, 57*). This reinforces our previous conclusion that the tryptophan residue in melittin is localized in a motionally restricted region when bound to membranes.

It is known that tryptophan has two overlapping $S_o \rightarrow S_1$ electronic transitions (^1L_a and ^1L_b) which are almost perpendicular to each other (*105–108*). Both $S_o \rightarrow {}^1L_a$ and $S_o \rightarrow {}^1L_b$ transitions occur in the 260–300 nm range. In nonpolar solvents, ^1L_a has higher energy than ^1L_b. However, in polar solvents, the energy level of ^1L_a is lowered, making it the lowest energy state. This inversion is believed to occur because ^1L_a transition has higher dipole moment (as it is directed through the ring -NH group), and can have dipole–dipole interactions with polar solvent molecules. Whether ^1L_a or ^1L_b is the lowest S_1 state, equilibration between these two states is believed to be very fast (of the order of 10^{-12} s), so that only emission from the lower S_1 state is observed (*109*). In a motionally restricted polar environment, absorption at the red edge photoselects the lowest energy S_1 (^1L_a in this case), and thus the polarization is high since only depolarization due to small angular differences between the absorption and emission transition moments and solvent reorientation, if any, occurs. Excitation at the shorter wavelengths, however, populates both ^1L_a and ^1L_b states. Equilibration between these two states produces a depolarization due to the approximately 90° angular difference between ^1L_a and ^1L_b moments. Thus, near 290 nm, there is a sharp dip in polarization due to maximal absorption by the ^1L_b state. Figure 3 shows such a characteristic dip around 290 nm in the excitation polarization spectrum of melittin in all cases (however, the dip is larger for DOPC). Thus, the sharp increase in polarization toward the red edge of the absorption band is probably because the extent of depolarization in melittin is reduced at the red edge not only due to decreased rotational rate of the fluorophore in the solvent relaxed state, but also due to photoselection of the predomi-

nantly ^1L_a transition, which in turn reduces the contribution to depolarization because of $^1L_b \rightarrow {}^1L_a$ equilibration.

The photoselection of the ^1L_a state toward the red edge could also account for the rather sharp change in the emission maximum with excitation wavelength for membrane-bound melittin, as is apparent from Figure 2. The excited state interactions with the solvent dipoles will be stronger for the ^1L_a state because of its higher dipole moment. This would enhance the extent of red shift in the emission maximum at higher excitation wavelengths.

Time-Resolved Fluorescence of Membrane-Bound Melittin

The origin of the red edge effect lies in differential extents of solvent reorientation around the excited state fluorophore, with each excitation wavelength selectively exciting a different average population of fluorophores (*46*). Since fluorescence lifetime serves as a faithful indicator for the local environment of a fluorophore and is known to be sensitive to excited state interactions, differential extents of solvent relaxation around a given fluorophore could be expected to give rise to differences in its lifetime. Table 2 shows the lifetimes of the tryptophan residue of melittin bound to different membrane types as a function of excitation wavelength, keeping the emission wavelength fixed at 350 nm. As can be seen from the table, when melittin in DOPC vesicles is excited at 294 nm, the decay fits a biexponential function, with the major component (pre-exponential factor 0.91) having a very short lifetime of 0.54 ns, and the minor component (pre-exponential factor 0.09) having a relatively longer lifetime of 3.86 ns. A typical decay profile with its biexponential fitting and the various statistical parameters used to check the goodness of the fit are shown in Figure 4.

When the excitation wavelength was gradually shifted from 294 to 316 nm, *i.e.*, toward the red edge of the absorption band, keeping the emission wavelength constant at 350 nm (see Table 2), it was found that the individual lifetimes did not change significantly. Interestingly, the pre-exponential factor for the short lifetime component shows a general increase with increasing excitation wavelength with
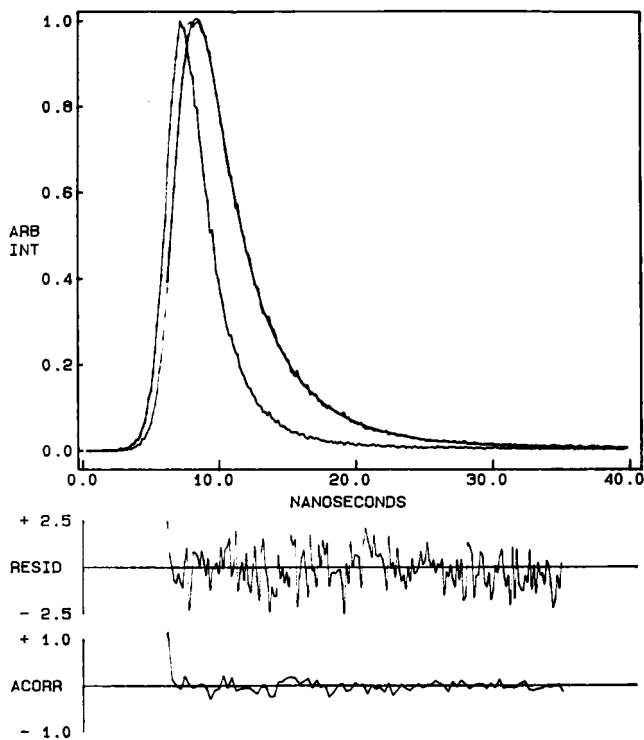
FIGURE 4: Time-resolved fluorescence intensity decay of melittin in SUVs of DOPC/DOPA. Excitation was at 296 nm, which corresponds to a peak in the spectral output of the nitrogen lamp. Emission was monitored at 370 nm. The sharp peak on the left is the lamp profile. The relatively broad peak on the right is the decay profile, fitted to a biexponential function. The two lower plots show the weighted residuals and the autocorrelation function of the weighted residuals. Melittin to lipid ratio was 1:50 (mol/mol). See Experimental Procedures for other details.

a concomitant reduction in the relatively long lifetime component. In order to confirm the above interpretation, the same set of fluorescence decays was subjected to global analysis. The decays were all assumed to be biexponential (on the basis of the results from discrete analysis), with lifetime components that were assumed to be linked among the data files and whose relative contributions (pre-exponential factors) were allowed to vary. The results of the global analysis are shown in parentheses in Table 2 and are found to be consistent with the above interpretation.

The mean fluorescence lifetimes of the tryptophan residue of membrane-bound melittin were calculated using eq 3 and are plotted as a function of excitation wavelength in Figure 5 for both discrete and global analysis (panels a and b). As shown in this figure, there is a steady decrease in the mean lifetime with increasing excitation wavelength from 294 to 316 nm, irrespective of the method of analysis (discrete or global). Such a marked shortening of lifetime at the red edge of the absorption band is indicative of slow solvent reorientation around the excited state fluorophore (*46*). The emission wavelength was set at 350 nm in order to avoid scattering artifacts at longer excitation wavelengths.

A careful examination of the data presented in Figure 5 and Table 2 shows that the decrease in the mean lifetime with red edge excitation is more for DOPC membranes (53%) than for membranes containing DOPC/DOPG (49%) or DOPC/DOPA (45%). It should be noted that these results are in agreement with the results from REES studies mentioned above (Table 1).

Table 3 shows the lifetimes of tryptophan residue of membrane-bound melittin as a function of emission wavelength, keeping the excitation wavelength constant at 296 nm. All decays corresponding to different emission wavelengths could be fitted to biexponential functions. Global analysis of this set of fluorescence decays was performed as mentioned above (assuming all decays to be biexponential with fixed lifetime components and varying pre-exponential factors) and the results are shown in parentheses in Table 3. The tryptophan residues exhibit two lifetimes at all the emission wavelengths studied, the major component (pre-exponential factor ∼0.9) having a lifetime of 0.29−1.15 ns, and the minor component (pre-exponential factor ∼0.1) having a lifetime of 3.04−5.75 ns. As the emission wavelength is gradually shifted from 330 to 380 nm, the pre-exponential factor corresponding to the short lifetime shows an overall decrease (accompanied by a simultaneous increase in the pre-exponential factor corresponding to the long lifetime) while the short lifetime component shows an overall increase.

The mean lifetimes, calculated using eq 3, are plotted as a function of emission wavelength in Figure 6 for both discrete and global analysis. As shown in this figure, there is a steady increase in the mean lifetime with increasing emission wavelength from 330 to 380 nm which is independent of the method of analysis (discrete or global). Such observation has been reported previously for fluorophores in environments of restricted mobility (*46*) as well as for membrane-bound melittin (*30*). Interestingly, in further agreement with the above results, the percent increase in the mean lifetime with increasing emission wavelength from 330 to 380 nm is more for zwitterionic membranes than for anionic membranes.

Polarization Changes with Emission Wavelength: A Novel Way To Monitor Motionally Restricted Environment

Fluorophores with longer lifetimes which emit at higher wavelengths should have more time to rotate in the excited state giving rise to lower polarization. Figure 7 shows the variation in steady state polarization of tryptophan residue of melittin bound to vesicles and in buffer, as a function of wavelength across its emission spectrum. As seen from the figure, while polarization values do not show any significant variation over the entire emission range in buffer, there is a considerable decrease in polarization with increasing emission wavelength in case of membrane-bound melittin. The lowest polarization is observed toward the red edge where the relaxed emission predominates. Similar observations have previously been reported for other membrane-bound fluorophores (*46*) as well as for melittin in reversed micelles (*110*).

A more quantitative analysis of Figure 7 in terms of the actual slopes of the plots brings out a novel point. The slopes for melittin bound to membranes of different charge types as well as in buffer, were determined by linear regression analysis of the plots ($r = 0.98−0.99$) and are shown in Table 4. As is evident from the table, the slope in case of melittin bound to zwitterionic DOPC is much greater than when bound to membranes containing negatively charged lipids (DOPC/DOPG or DOPC/DOPA membranes). This clearly shows that such variation in slopes can reflect relative
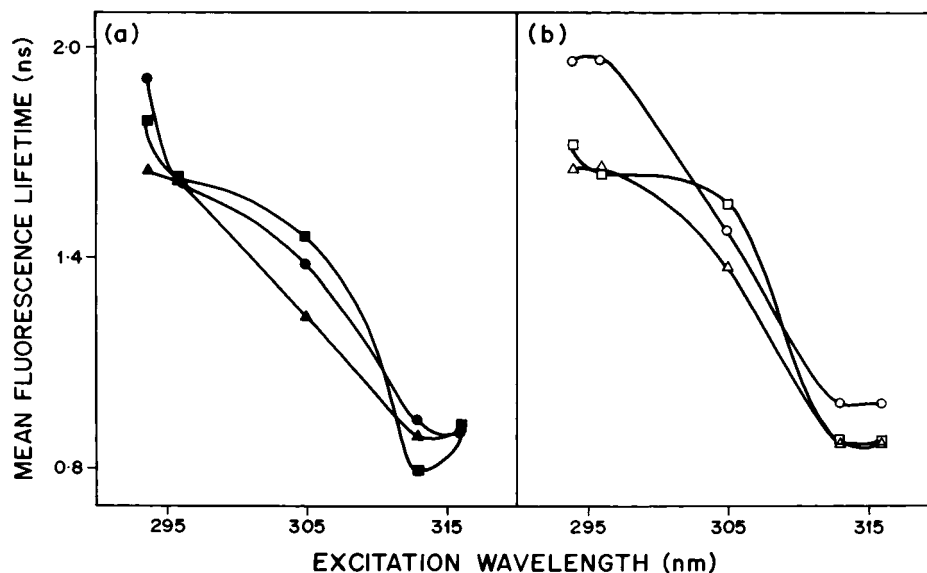
FIGURE 5: Mean fluorescence lifetime of membrane-bound melittin as a function of excitation wavelength. Emission wavelength was kept constant at 350 nm. Mean lifetimes were calculated from Table 2 using eq 3. The fluorescence lifetimes were analyzed using (a) the discrete analysis for vesicles of DOPC (●), DOPC/DOPG (■), and DOPC/DOPA (▲) and (b) global analysis for vesicles of DOPC (○), DOPC/DOPG (□), and DOPC/DOPA (△). Melittin to lipid ratio was 1:50 (mol/mol). See Experimental Procedures for other details.

Table 3: Lifetimes of Membrane-Bound Melittin as Functions of Emission Wavelength[a]

emission wavelength (nm)	α_1	τ_1 (ns)	α_2	τ_2 (ns)
(a) DOPC				
330	0.98 (0.97)[b]	0.65 (0.48)	0.02 (0.03)	4.94 (3.79)
334	0.96 (0.96)	0.54 (0.48)	0.04 (0.04)	4.20 (3.79)
340	0.94 (0.95)	0.60 (0.48)	0.06 (0.05)	3.83 (3.79)
350	0.95 (0.92)	0.29 (0.48)	0.05 (0.08)	3.62 (3.79)
360	0.89 (0.91)	0.61 (0.48)	0.11 (0.09)	3.88 (3.79)
370	0.85 (0.87)	0.80 (0.48)	0.15 (0.13)	4.51 (3.79)
380	0.82 (0.83)	0.87 (0.48)	0.18 (0.17)	4.60 (3.79)
(b) DOPC/DOPG				
330	0.98 (0.96)	0.69 (0.59)	0.02 (0.04)	5.39 (3.40)
334	0.96 (0.95)	0.60 (0.59)	0.04 (0.05)	3.98 (3.40)
340	0.92 (0.93)	0.60 (0.59)	0.08 (0.07)	3.32 (3.40)
350	0.89 (0.90)	0.54 (0.59)	0.11 (0.10)	3.11 (3.40)
360	0.87 (0.89)	0.54 (0.59)	0.13 (0.11)	3.04 (3.40)
370	0.84 (0.85)	1.01 (0.59)	0.16 (0.15)	3.91 (3.40)
380	0.82 (0.82)	1.11 (0.59)	0.18 (0.18)	4.08 (3.40)
(c) DOPC/DOPA				
330	0.99 (0.97)	0.54 (0.60)	0.01 (0.03)	5.75 (3.47)
334	0.96 (0.95)	0.60 (0.60)	0.04 (0.05)	3.68 (3.47)
340	0.92 (0.94)	0.53 (0.60)	0.08 (0.06)	3.06 (3.47)
350	0.90 (0.91)	0.60 (0.60)	0.10 (0.09)	3.30 (3.47)
360	0.87 (0.89)	0.60 (0.60)	0.13 (0.11)	3.21 (3.47)
370	0.85 (0.86)	1.01 (0.60)	0.15 (0.14)	3.99 (3.47)
380	0.84 (0.85)	1.15 (0.60)	0.16 (0.15)	4.12 (3.47)

[a] Excitation wavelength 296 nm. [b] Numbers in parentheses are the results of global analysis.

difference in restriction experienced by the fluorophore in its local environment. Thus, the slope for melittin bound to DOPC vesicles, where a REES of 5 nm is observed (Table 1), is greater than the slope obtained for melittin incorporated in either DOPC/DOPG or DOPC/DOPA vesicles, for which a REES of 2−3 nm is observed (see Table 4). This is further supported by the low value of the slope obtained for melittin in buffer which is much lower than what is obtained in any of the membrane systems. It is noteworthy that monomeric melittin in buffer does not exhibit any REES (Table 1).

Near- and Far-UV CD Spectra of Membrane-Bound Melittin

The far- and near-UV CD spectra of monomeric melittin in buffer and bound to vesicles of DOPC and DOPC/DOPG are shown in Figure 8. Figure 8a shows the far-UV (205−250 nm) CD spectra of melittin and is indicative of the secondary structure of melittin under various conditions. While aqueous melittin shows essentially random secondary structure, the spectra of melittin bound to vesicles are characteristics of peptides in helical conformation. The spectra of melittin bound to zwitterionic DOPC or to membranes containing negative charge (such as DOPC/DOPG vesicles) are similar indicating that there is no significant change in secondary structure in these two cases.

In contrast to the far-UV CD spectrum which provides information about secondary structure, information regarding the tertiary structure can be obtained from the near-UV CD spectrum. Furthermore, since melittin has only one tryptophan residue and has no other aromatic amino acid residue (which could absorb in the near-UV range), the CD signal in the near-UV region is dominated by the sole tryptophan and any difference in near-UV CD spectra can be correlated to the difference in tryptophan environments experienced in different membranes. The changes in tertiary structure (with respect to tryptophan) of melittin bound to DOPC and DOPC/DOPG vesicles were thus analyzed by near-UV (260−315 nm) CD spectra (see Figure 8b). The near-UV CD spectrum of membrane-bound melittin has a characteristic appearance depending on the type of vesicle used. Melittin in DOPC vesicles shows a band of positive ellipticity around 290 nm. In contrast to this, a band of positive ellipticity around 270 nm is observed for melittin in DOPC/DOPG vesicles. We attribute the 270 nm band to the L_a band and the 290 nm band to the L_b band of tryptophan (111). It is worth recalling here that it is the energy of the L_a band that is very sensitive to the environment due to the large change in dipole moment upon excitation (105). Thus, while the L_b transition is predominant for melittin bound to DOPC vesicles, it is the L_a transition that is more intense in vesicles containing
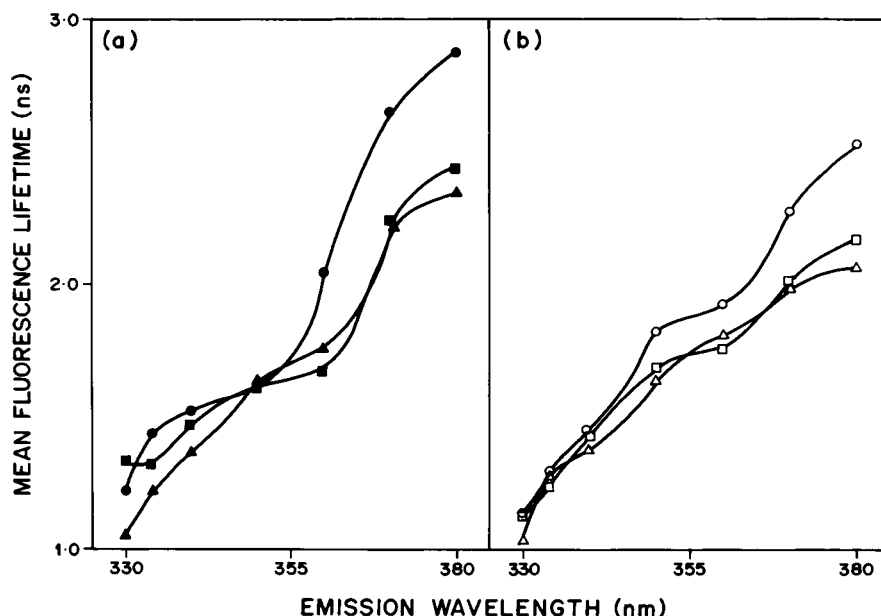
FIGURE 6: Mean fluorescence lifetime of membrane-bound melittin as a function of emission wavelength. Excitation wavelength was kept constant at 296 nm. Mean lifetimes were calculated from Table 3 using eq 3. The fluorescence lifetimes were analyzed using (a) the discrete analysis for vesicles of DOPC (●), DOPC/DOPG (■), and DOPC/DOPA (▲) and (b) global analysis for vesicles of DOPC (○), DOPC/DOPG (□), and DOPC/DOPA (△). Melittin to lipid ratio was 1:50 (mol/mol). See Experimental Procedures for other details.
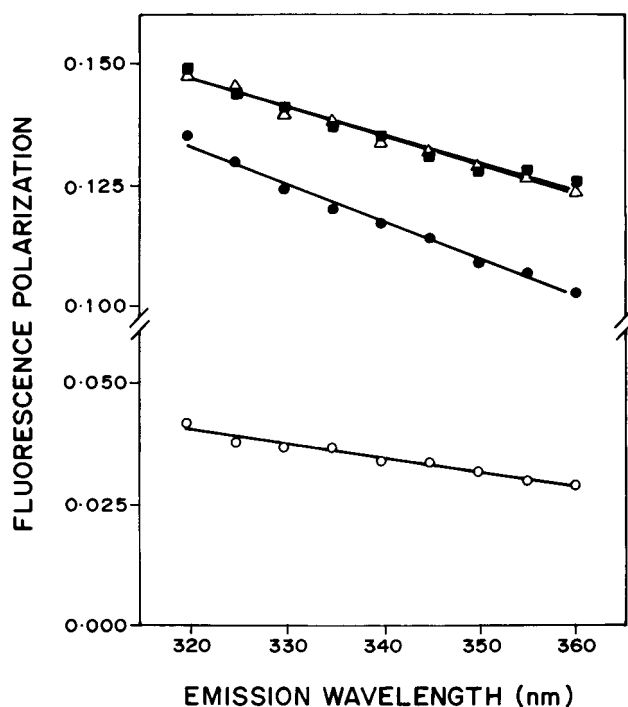

FIGURE 7: Fluorescence polarization of melittin as a function of emission wavelength in buffer (○) and vesicles of DOPC (●), DOPC/DOPG (■), and DOPC/DOPA (△). The excitation wavelength was 280 nm. Melittin to lipid ratio was 1:50 (mol/mol) in different vesicles. The concentration of melittin in buffer was 8.53 μM. See Experimental Procedures for other details.

negatively charged lipids, *i.e.*, in the DOPC/DOPG vesicle system. Melittin bound to DOPC/DOPA vesicles also exhibits intense L_a transition (data not shown). It is interesting to note here that this result is in agreement with our results of fluorescence polarization with increasing excitation wavelength (see above) where it was observed that the characteristic dip in polarization around 290 nm (due to maximal absorption by the L_b state) was more for melittin in DOPC vesicles (see Figure 3). It is thus clear from the near-UV CD spectra of membrane-bound melittin that the

Table 4: Fluorescence Polarization of Melittin in Different Environments[a]

medium	composition	polarization (P)	slope of P vs emission[b] wavelength ($\times 10^4$) (nm^{-1})	r^c
membrane				
zwitterionic	DOPC	0.122	7.77	0.99
anionic	DOPC/DOPG	0.138	5.73	0.98
anionic	DOPC/DOPA	0.138	5.93	0.99
buffer	10 mM MOPS 150 mM NaCl 5 mM EDTA, pH 7.0	0.037	2.97	0.98

[a] Samples were excited at 280 nm and emission was collected at 334 nm. [b] From Figure 7 by linear regression analysis. [c] r is the correlation coefficient.

tryptophan experiences different environments when bound to zwitterionic as opposed to negatively charged membranes. This difference in environment could account for the difference in activity of membrane-bound melittin in these two cases (see Figure 1) since the sole tryptophan residue has been shown to be crucial for the activity of the peptide (*39–42*).

Tryptophan Depth in Membrane-Bound Melittin

Membrane penetration depth is an important parameter in the study of membrane structure and organization (*112, 113*). Knowledge of the precise depth of a membrane embedded group or molecule often helps define the conformation and topology of membrane proteins and peptides. In addition, properties such as polarity, fluidity, segmental motion, ability to form hydrogen bonds, and the extent of solvent penetration are known to vary in a depth dependent manner. In order to gain a better understanding of melittin−membrane interactions, especially in terms of interaction of melittin with membranes of different charge types, penetration depths of the sole tryptophan residue of melittin in membranes were
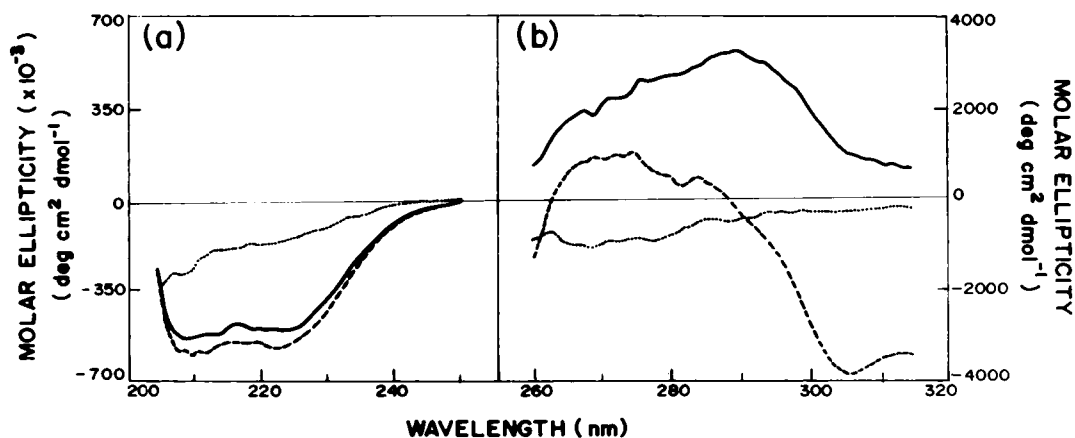
FIGURE 8: Far-UV (a) and near-UV (b) CD spectra of melittin in buffer (···) and in vesicles of DOPC (—) and DOPC/DOPG (- - -). The concentration of melittin was 34.17 μM in all cases. Melittin to lipid ratio was 1:50 (mol/mol). See Experimental Procedures for other details.

Table 5: Penetration Depth of the Tryptophan in Membrane-Bound Melittin by the Parallax Method[a]

membrane type	composition	distance from the center of the bilayer z_{cF} (Å)
zwitterionic	DOPC	10.6
anionic	DOPC/DOPG	10.9

[a] Depths were calculated from fluorescence quenchings obtained with samples containing 15 mol % of 5-PC and 12-PC and using eq 5. Samples were excited at 280 nm, and emission was collected at 334 nm.

determined. Depth of the tryptophan residue in membrane-bound melittin was calculated by the parallax method (*72*) using the equation

$$z_{cF} = L_{c1} + \{[(-1/\pi C)\ln(F_1/F_2) - L_{21}^2]/2L_{21}\} \quad (5)$$

where z_{cF} = the depth of the fluorophore from the center of the bilayer, L_{c1} = the distance of the center of the bilayer from the shallow quencher (5-PC in this case), L_{21} = the difference in depth between the two quenchers (*i.e.*, the transverse distance between the shallow and the deep quencher), and C = the two-dimensional quencher concentration in the plane of the membrane (molecules/Å^2). Here F_1/F_2 is the ratio of F_1/F_o and F_2/F_o in which F_1 and F_2 are fluorescence intensities in the presence of the shallow and deep quencher, respectively, both at the same quencher concentration C; F_o is the fluorescence intensity in the absence of any quencher. All the bilayer parameters used were the same as described previously (*72*). The depths of penetration of the tryptophan residue for melittin bound to zwitterionic (DOPC) and anionic (DOPC/DOPG) membranes are shown in Table 5 and are found to be located at 10.6 and 10.9 Å from the center of the bilayer, respectively. This is in agreement with tryptophan depth in membrane-bound melittin determined by fluorescence quenching using brominated phospholipids (*114*). These depth values indicate that the tryptophan residue is located at a shallow interfacial region of the membrane as has been previously observed with membrane embedded tryptophans of other membrane proteins and peptides (*60, 115−119*). These include magainin 2, another cationic peptide isolated from frog skin that has antibacterial activity (*120*). Further, the penetration depths of the membrane-embedded tryptophan in membranes of different surface charges are not significantly different.

DISCUSSION

Anionic phospholipids play a major role in lipid−protein interactions, and in membrane insertion and translocation of proteins (*121−126*). Approximately 30% of the total phospholipids in eukaryotic cell membranes contain negatively charged head groups (*122*). In the plasma membrane, these acidic phospholipids are localized predominantly in the inner leaflet of the bilayer, imparting a negative charge to the cytoplasmic surface of the cell. The classic example of this type of asymmetry is found in the red blood cell membranes where the negatively charged phosphatidylserines are localized in the inner leaflet of the bilayer (*127*). Membrane proteins such as MARCKS, protein kinase C, and the Src family of tyrosine protein kinases have been shown to have clusters of basic amino acids that interact electrostatically with negatively charged phospholipids (*122*). These proteins are cytosolic in nature, and reversibly associate with the cytoplasmic face of the plasma membrane in order to initiate cellular signaling events (*121, 122*). The electrostatic interaction between their basic patch and the negatively charged phospholipids contributes considerable membrane binding energy to stabilize their interaction with membranes (*128*). Such charge-dependent membrane binding often leads to domain formation at the membrane interface triggered by lipid−protein interaction (*99, 129*).

In this paper, we have utilized the wavelength-selective fluorescence approach to monitor the modulation of the tryptophan environment of membrane-bound melittin by lipids of different charge types. We observe a REES of 2−3 nm for the tryptophan of melittin when bound to negatively charged membranes, depending on the type and relative amount of the anionic lipid used. On the other hand, in case of melittin bound to membranes composed of zwitterionic lipids, we observe a REES of 5 nm, in agreement with our previous results (*36*). This reduction in the magnitude of REES in case of negatively charged membranes signifies relatively less restriction to solvent reorientation, and points out that the wavelength-selective fluorescence approach is sensitive to such changes in lipid−peptide interactions brought about by electrostatics. This is further supported by studies in which fluorescence polarization of melittin was monitored as a function of emission wavelength. Emission wavelength dependence of polarization shows characteristic differences for membranes containing zwitterionic and negatively charged lipids (Table 4). To the best of our
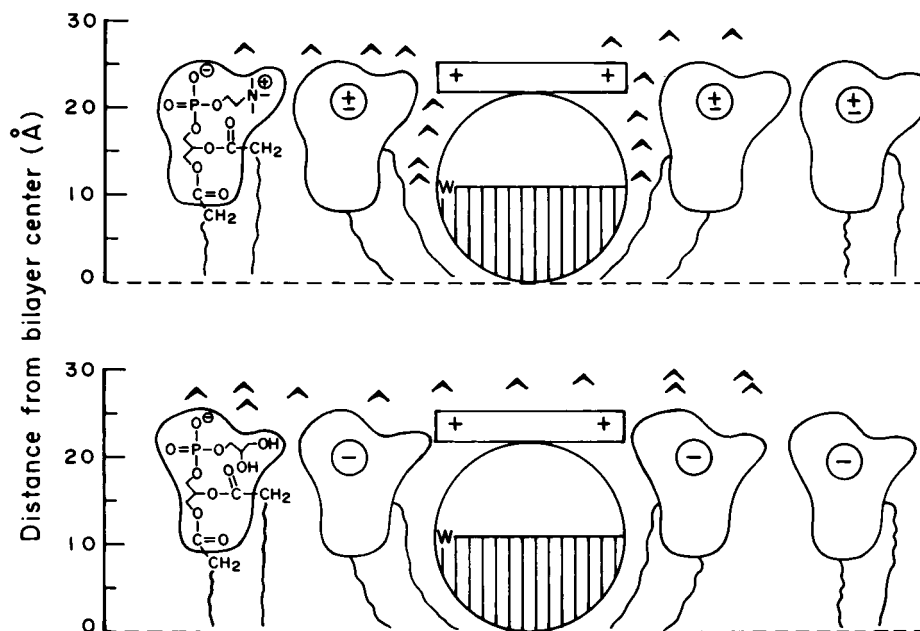
FIGURE 9: Schematic representation of the membrane bilayer showing the orientation and location of melittin. Two types of membranes are shown: zwitterionic (upper panel) and anionic (lower panel) membranes. The shaded region represents the hydrophobic face of the amphiphilic helix formed by membrane-bound melittin with the tryptophan residue (W) at the interface of the hydrophobic and the hydrophilic regions of the amphiphilic helix. The tryptophan residue is localized at comparable depths in both cases (Table 5). The peptide orientation is shown parallel to the membrane surface (*13*) with the hydrophobic face directed toward the membrane interior (*145*). The last few residues (residues 23−26) that are not part of the helix (*145*) are shown separately in the rectangle. The effective charge of the membrane-bound peptide under similar conditions has been shown to be +2 after appropriate corrections are made for electrostatic effects (*146*). This is shown in the rectangle. The shaded open triangles (ˆ) represent interfacial (membrane associated) water molecules. The dotted line indicates the center of the bilayer. See text for other details.

knowledge, this is the first report demonstrating that the slopes of fluorescence polarization *vs* emission wavelength plots provide important information regarding differences in restriction of a fluorophore present in different environments due to alteration of solvent reorientation dynamics.

Time-resolved fluorescence measurements of melittin provide further insight into organization of melittin in membranes. The mean fluorescence lifetime of monomeric melittin in aqueous buffer is ∼1.85 ns when emission is collected at 330 nm corresponding to excitation at 296 nm (data not shown), in agreement with previous literature value (*130*). When incorporated into membranes of DOPC, the lifetime is reduced to 1.23 ns (Table 3 and Figure 6) along with a slight reduction in fluorescence intensity. This is surprising since the tryptophan lifetimes are generally shorter in polar solvents due to fast deactivating processes (*131*). However, the shortening of the lifetime could be due to steric interaction between Trp-19 and Lys-23 which will be in close proximity in a helical arrangement (*35*). Since Lys-23 in melittin has a pK_a of 8.6 (*132*), it will be positively charged at physiological pH. Interestingly, only the protonated, positively charged form of the amino group is believed to be an efficient quencher of tryptophan fluorescence (*35*) which is seen as a reduction in fluorescence intensity and lifetime when melittin is incorporated into membranes from aqueous solution. In more general terms, such interactions can be classified as cation−π interactions which have recently been shown to play an important role in biology (*133*, *134*).

The far-UV CD spectra of melittin bound to zwitterionic (DOPC) and anionic (DOPC/DOPG) vesicles are similar indicating no major change in the peptide backbone arrangement. Although the far-UV CD spectra of membrane-bound

melittin have been previously reported by various groups (*11−13*), this is the first report describing the near-UV CD spectra of membrane-bound melittin. The near-UV CD spectra of melittin bound to zwitterionic and anionic membranes showed major differences in band positions thereby providing a strong evidence about the difference in tryptophan environments which could be responsible for the modulation of lytic activity in these two cases.

The location of the sole tryptophan in membrane-bound melittin was previously investigated from fluorescence quenching by water soluble quenchers such as acrylamide (*30*, *31*), iodide, and nitrate ions (*31*), as well as by brominated (*31*) or spin-labeled (*29*) fatty acids. While quenching by aqueous quenchers provides an idea about the degree of accessibility from the aqueous solution, it cannot pinpoint the true location (depth) of the membrane-bound fluorophore. On the other hand, there are several limitations in using fatty acid probes as lipid analogues in quenching studies, as outlined in the following points: (i) spin-labeled fatty acids are not firmly held in one position in relation to the bilayer; instead, they appear to exhibit marked vertical fluctuations as detected by electron−electron double-resonance studies (*135*, *136*); (ii) free fatty acids are not normal membrane components, and when used in high concentrations (as is often required in quenching studies), they may exert the lytic effects of detergents; (iii) the possibility of varying degrees of ionization of fatty acid probes should be taken into consideration. The degree of ionization varies with pH, and consequently, the location of these probes in the bilayer may be pH dependent (*79*, *137*); (iv) fatty acids are much more water soluble than lipids, and some of the labeled fatty acid will partition into the aqueous phase. This partitioning depends on the attachment site of

the spin-label group in the acyl chain (*138*). Anomalous quenching of anthroyloxy probes has been attributed to this type of complication (*139*); and (v) fatty acids have been shown to perturb structure and function of membrane proteins (*140*, *141*). This is significant in this case since it has been shown that fatty acids affect lytic activity of melittin (*70*). In the present study, we have used spin-labeled phospholipids (rather than fatty acids) with the nitroxide group attached to different positions of the fatty acyl chain. Further, we have used the parallax method for measurement of membrane penetration depth which allows direct determination of depth in angstroms (*72*). Since melittin has only one tryptophan, the interpretation of depth values thus obtained is devoid of complications that often arise for depth analysis of multit-ryptophan proteins (*116*). Our results show that there is no appreciable difference in tryptophan depths for melittin bound to zwitterionic and anionic membranes.

The interaction of melittin with membranes of different charge types has important functional consequence. For example, it has been shown by us (Figure 1) and other groups (*69*−*71*) that the presence of negatively charged lipids inhibits membrane lysis induced by melittin and this inhibition increases with increasing charge density in the membrane. The modulation of the lytic effect is believed to originate from the electrostatic interaction between the peptide and the membrane surface (see Figure 9). The binding of melittin to charged membranes is 2 orders of magnitude stronger than membranes containing only zwitterionic phospholipids (*65*). It is thus likely that electrostatic interactions between the positively charged peptide and the negatively charged lipid head groups play an important role in modulating the lytic activity. As is schematically shown in Figure 9, in case of zwitterionic membranes (upper panel), the predominant driving force for the peptide−membrane interaction will be the interaction of the hydrophobic fatty acyl chains with the apolar face of the melittin amphiphilic helix. The lack of specific (electrostatic) interaction between the peptide and the lipid head group leads to penetration of the interfacial water in the membrane interior thereby allowing such water molecules in the proximity of the tryptophan residue. Such interfacial water molecules will be motionally restricted (*142*, *143*), giving rise to a REES of 5 nm (Table 1). In case of anionic membranes (lower panel), the major driving force for peptide−membrane interaction will be the favorable electrostatic interaction between the negatively charged lipid head group and the positively charged residues of the peptide. The close interaction of the charged peptide with the oppositely charged lipid head group results in poor water penetration in the membrane interior, especially around the interfacial tryptophan residues. This results in a relatively nonpolar environment around the tryptophan in negatively charged vesicles leading to a blue shift (1−2 nm) of the fluorescence emission maximum compared to zwitterionic vesicles, and a reduction in REES to 2−3 nm (as opposed to 5 nm for zwitterionic membranes).

The mechanism of membrane lysis by melittin is thought to involve two steps: (i) interaction of melittin with the membrane surface leading to partial insertion into the interfacial region, and (ii) redistribution of the peptide in the lipid assembly leading to disruption of the membrane (*70*). The second step, whose mechanism is not known, requires the peptide to be transferred to the apolar region of

the membrane. It is this step that is inhibited by negatively charged lipids because of stronger electrostatic interaction leading to inhibition of lytic activity. This is significant in the context of high hemolytic activity of melittin. In the red blood cell membrane, as mentioned above, the distribution of lipids in the two leaflets is such that the zwitterionic phospholipids such as phosphatidylcholine and sphingomyelin are mostly present in the outer leaflet of the bilayer while the negatively charged phophatidylserine is present exclusively in the inner leaflet (*127*). It is important to note here that for its natural hemolytic activity, melittin has to approach the target membrane from the outside of the membrane, and thus the lipids it immediately interacts with are zwitterionic in nature (*38*). Our results presented here on the environment of the tryptophan, a residue shown to be crucial for hemolytic activity (*39*−*42*), of membrane-bound melittin for membranes of different charge types, as monitored by the wavelength-selective fluorescence approach, provide further insight into molecular details of the process. More importantly, our results are relevant in the general context of interaction of membrane-active, amphiphilic peptides such as magainins, cecropins, paradaxin (*7*), and indolicidin (*144*) with the membrane bilayer.

ACKNOWLEDGMENT

REFERENCES

1. Habermann, E., and Jentsch, J. (1967) *Hoppe-Seyler's Z. Physiol. Chem. 248*, 37−50.
2. Habermann, E. (1972) *Science 177*, 314−322.
3. Dufourcq, J., Dasseux, J. L., and Faucon, J. F. (1984) in *Bacterial Protein Toxins* (Alouf, J. E., Fehrenbach, F. J., Freer, J. H., and Jeljaszewicz, J., Eds.) pp 127−138, Academic Press, London.
4. Bernheimer, A. W., and Rudy, B. (1986) *Biochim. Biophys. Acta 864*, 123−141.
5. Dempsey, C. E. (1990) *Biochim. Biophys. Acta 1031*, 143−161.
6. Sansom, M. S. P. (1991) *Prog. Biophys. Mol. Biol. 55*, 139−235.
7. Saberwal, G., and Nagaraj, R. (1994) *Biochim. Biophys. Acta 1197*, 109−131.
8. Shai, Y. (1995) *Trends Biochem. Sci. 20*, 460−464.
9. Bechinger, B. (1997) *J. Membr. Biol. 156*, 197−211.
10. Bello, J., Bello, H. R., and Granados, E. (1982) *Biochemistry 21*, 461−465.
11. Knoppel, E., Eisenberg, D., and Wickner, W. (1979) *Biochemistry 18*, 4177−4181.
12. Chandani, B., and Balasubramanian, D. (1986) *Biopolymers 25*, 1259−1272.
13. De Jongh, H. H. J., Goormaghtigh, E., and Killian, J. A. (1994) *Biochemistry 33*, 14521−14528.
14. Terwilliger, T. C., and Eisenberg, D. (1982) *J. Biol. Chem. 237*, 6016−6022.
15. Degrado, W. F., Musso, G. F., Lieber, M., Kaiser, E. T., and Kezdy, F. J. (1982) *Biophys. J. 37*, 329−338.
16. Kaiser, E. T., and Kezdy, F. J. (1983) *Proc. Natl. Acad. Sci. U.S.A. 80*, 1137−1143.
17. Morii, H., Honda, S., Ohashi, S., and Uedaira, H. (1994) *Biopolymers 34*, 481−488.
18. Garnier, J., Gaye, P., Mercier, J.-C., and Robson, B. (1980) *Biochimie 62*, 231−239.

19. Golding, C., and O'Shea, P. (1995) *Biochem. Soc. Trans. 23*, 971−976.
20. Eisenberg, D., and Wesson, M. (1990) *Biopolymers 29*, 171−177.
21. Rabenstein, M., and Shin, Y.-K. (1995) *Biochemistry 34*, 13390−13397.
22. Leippe, M., Ebel, S., Schoenberger, O. L., Horstmann, R. D., and Muller-Eberhard, H. J. (1991) *Proc. Natl. Acad. Sci. U.S.A. 88*, 7659−7663.
23. Leippe, M., Tannich, E., Nickel, R., van der Goot, G., Pattus, F., Horstmann, R. D., and Muller-Eberhard, H. J. (1992) *EMBO J. 11*, 3501−3506.
24. Clague, M. J., and Cherry R. J. (1988) *Biochem. J. 252*, 791−794.
25. Hermetter, A., and Lakowicz, J. R. (1986) *J. Biol. Chem. 261*, 8243−8248.
26. Talbot, J. C., Faucon J. F., and Dufourcq, J. (1987) *Eur. Biophys. J. 15*, 147−157.
27. Altenbach, C., and Hubbell, W. L. (1988) *Proteins 3*, 230−242.
28. John, E., and Jahnig, F. (1991) *Biophys. J. 60*, 319−328.
29. Vogel, H. (1981) *FEBS Lett. 134*, 37−42.
30. Georghiou, S., Thompson, M., and Mukhopadhyay, A. K. (1982) *Biochim. Biophys. Acta 688*, 441−452.
31. Batenburg, A. M., Hibbeln, J. C. L., and De Kruijff, B. (1987) *Biochim. Biophys. Acta 903*, 155−165.
32. Frey, S., and Tamm, L. K. (1991) *Biophys. J. 60*, 922−930.
33. Bradrick, T. D., Philippetis, A., and Georghiou, S. (1995) *Biophys. J. 69*, 1999−2010.
34. Dufourcq, J., and Faucon, J.-F. (1977) *Biochim. Biophys. Acta 467*, 1−11.
35. Weaver, A. J., Kemple, M. D., Brauner, J. W., Mendelsohn, R., and Prendergast, F. G. (1992) *Biochemistery 31*, 1301−1313.
36. Chattopadhyay, A., and Rukmini, R. (1993) *FEBS Lett. 335*, 341−344.
37. Cajal, Y., and Jain, M. K. (1997) *Biochemistry 36*, 3882−3893.
38. Oren, Z., and Shai, Y. (1997) *Biochemistry 36*, 1826−1835.
39. Habermann, E., and Kowallek, H. (1970) *Hoppe-Seyler's Z. Physiol. Chem. 351*, 884−890.
40. Blondelle, S. E., and Houghten, R. A. (1991) *Peptide Res. 4*, 12−18.
41. Blondelle, S. E., and Houghten, R. A. (1991) *Biochemistry 30*, 4671−4678.
42. Blondelle, S. E., Simpkins, L. R., Perez-Paya, E., and Houghten, R. A. (1993) *Biochim. Biophys. Acta 1202*, 331−336.
43. Perez-Paya, E., Houghten, R. A., and Blondelle, S. E. (1994) *Biochem. J. 299*, 587−591.
44. Perez-Paya, E., Houghten, R. A., and Blondelle, S. E. (1995) *J. Biol. Chem. 270*, 1048−1056.
45. Hewish, D., Werkmeister, J., Kirkpatrick, A., Curtain, C., Pantela, G., and Rivett, D. E. (1996) *J. Protein Chem. 15*, 395−403.
46. Mukherjee, S., and Chattopadhyay, A. (1995) *J. Fluoresc. 5*, 237−246.
47. Galley, W. C., and Purkey, R. M. (1970) *Proc. Natl. Acad. Sci. U.S.A. 67*, 1116−1121.
48. Lakowicz, J. R., and Keating-Nakamoto, S. (1984) *Biochemistry 23*, 3013−3021.
49. Demchenko, A. P. (1988) *Trends Biochem. Sci. 13*, 374−377.
50. Haussinger, D. (1996) *Biochem. J. 313*, 697−710.
51. Ho, C., and Stubbs, C. D. (1992) *Biophys. J. 63*, 897−902.
52. Fischer, W. B., Sonar, S., Marti, T., Khorana, H. G., and Rothschild, K. J. (1994) *Biochemistry 33*, 12757−12762.
53. Kandori, H., Yamazaki, Y., Sasaki, J., Needleman, R., Lanyi, J. K., and Maeda, A. (1995) *J. Am. Chem. Soc. 117*, 2118−2119.
54. Sankararamakrishnan, R., and Sansom, M. S. P. (1995) *FEBS Lett. 377*, 377−382.
55. Chattopadhyay, A. (1991) *Biophys. J. 59*, 191a.
56. Chattopadhyay, A., and Mukherjee, S. (1993) *Biochemistry 32*, 3804−3811.
57. Mukherjee, S., and Chattopadhyay, A. (1994) *Biochemistry 33*, 5089−5097.
58. Mukherjee, S., Chattopadhyay, A., Samanta, A., and Soujanya, T. (1994) *J. Phys. Chem. 98*, 2809−2812.
59. Guha, S., Rawat, S. S., Chattopadhyay, A., and Bhattacharyya, B. (1996) *Biochemistry 35*, 13426−13433.
60. Chattopadhyay, A., Mukherjee, S., Rukmini, R., Rawat, S. S., and Sudha, S. (1997) *Biophys. J. 73*, 839−849.
61. Rawat, S. S., Mukherjee, S., and Chattopadhyay, A. (1997) *J. Phys. Chem. B 101*, 1922−1929.
62. Bernard, E., Faucon, J.-F., and Dufourcq, J. (1982) *Biochim. Biophys. Acta 688*, 152−162.
63. Beschiaschvili, G., and Seelig, J. (1990) *Biochemistry 29*, 52−58.
64. Kleinschmidt, J. H., Mahaney, J. E., Thomas, D. D., and Marsh, D. (1997) *Biophys. J. 72*, 767−778.
65. Batenburg, A. M., Van Esch, J. H., and De Kruijff, B. (1988) *Biochemistry 27*, 2324−2331.
66. Batenburg, A. M., Hibbeln, J. C. L., Verkleij, A. J., and De Kruijff, B. (1987) *Biochim. Biophys. Acta 903*, 142−154.
67. Batenburg, A. M., Van Esch. J. H., Leunissen-Bijvelt, J., Verkleij, A. J., and De Kruijff, B. (1987) *FEBS Lett. 223*, 148−154.
68. Batenburg, A. M., and De Kruijff, B. (1988) *Biosci. Rep. 8*, 299−307.
69. Benachir, T., and Lafleur, M. (1995) *Biochim. Biophys. Acta 1235*, 452−460.
70. Monette, M., and Lafleur, M. (1995) *Biophys. J. 68*, 187−195.
71. Hincha, D. K., and Crowe, J. H. (1996) *Biochim. Biophys. Acta 1284*, 162−170.
72. Chattopadhyay, A., and London, E. (1987) *Biochemistry 26*, 39−45.
73. Dittmer, J. C., and Lester, R. L. (1964) *J. Lipid. Res. 5*, 126−127.
74. McClare, C. W. F. (1971) *Anal. Biochem. 39*, 527−530.
75. Quay, S. C., and Condie, C. C. (1983) *Biochemistry 22*, 695−700.
76. Argiolas, A., and Pisano, J. J. (1983) *J. Biol. Chem. 258*, 13697−13702.
77. Asuncion-Punzalan, E., and London, E. (1995) *Biochemistry 34*, 11460−11466.
78. Abrams, F. S., and London, E. (1993) *Biochemistry 32*, 10826−10831.
79. Abrams, F. S., Chattopadhyay, A., and London, E. (1992) *Biochemistry 31*, 5322−5327.
80. Batzri, S., and Korn, E. D. (1973) *Biochim. Biophys. Acta 298*, 1015−1019.
81. Kremer, J. M. H., Esker, M. W. J., Pathmamanoharan, C., and Wiersema, P. H. (1977) *Biochemistry 16*, 3932−3935.
82. Chen, R. F., and Bowman, R. L. (1965) *Science 147*, 729−732.
83. Bevington, P. R. (1969) *Data Reduction and Error Analysis for the Physical Sciences*, McGraw-Hill, New York.
84. O'Connor, D. V., and Phillips, D. (1984) in *Time-Correlated Single Photon Counting*, pp 180−189, Academic Press, London.
85. Lampert, R. A., Chewter, L. A., Phillips, D., O'Connor, D. V., Roberts, A. J., and Meech, S. R. (1983) *Anal. Chem. 55*, 68−73.
86. Grinvald, A., and Steinberg, I. Z. (1974) *Anal. Biochem. 59*, 583−598.
87. Lakowicz, J. R. (1983) *Principles of Fluorescence Spectroscopy*, Plenum Press, New York.
88. Knutson, J. R., Beechem, J. M., and Brand, L. (1983) *Chem. Phys. Lett. 102*, 501−507.
89. Beechem, J. M. (1989) *Chem. Phys. Lipids 50*, 237−251.
90. Beechem, J. M., Gratton, E., Ameloot, M., Knutson, J. R., and Brand, L. (1991) in *Topics in Fluorescence Spectroscopy, Vol. 2: Principles* (Lakowicz, J. R., Ed.) pp 241−305, Plenum Press, New York.
91. Beechem, J. M. (1992) *Methods Enzymol. 210*, 37−54.
92. Chen, G. C., and Yang, J. T. (1977) *Anal. Lett. 10*, 1195−1207.
93. Weinstein, J. N., Yoshikami, S., Henkart, P., Blumenthal, R., and Hagins, W.A. (1977) *Science 195*, 489−492.
94. Stewart, J. C. M. (1980) *Anal. Biochem. 104*, 10−14.
95. Chattopadhyay, A. (1990) *Chem. Phys. Lipids 53*, 1−15.

96. Perochon, E., Lopez, A., and Tocanne, J. F. (1992) *Biochemistry 31*, 7672−7682.
97. Slater, S. J., Ho, C., Taddeo, F. J., Kelly, M. B., and Stubbs, C. D. (1993) *Biochemistry 32*, 3714−3721.
98. Venable, R. M., Zhang, Y., Hardy, B. J., and Pastor, R. W. (1993) *Science 262*, 223−226.
99. Gawrisch, K., Barry, J. A., Holte, L. L., Sinnwell, T., Bergelson, L. D., and Ferretti, J. A. (1995) *Mol. Membr. Biol. 12*, 83−88.
100. Ashcroft, R. G., Coster, H. G. L., and Smith, J. R. (1981) *Biochim. Biophys. Acta 643*, 191−204.
101. Yeagle, P. (1987) in *The Membranes of Cells*, pp 89−90, Academic Press, Orlando, FL.
102. Boggs, J. M. (1987) *Biochim. Biophys. Acta 906*, 353−404.
103. Shin, T.-B., Leventis, R., and Silvius, J. R. (1991) *Biochemistry 30*, 7491−7497.
104. Itoh, K.-I., and Azumi, T. (1975) *J. Chem. Phys. 62*, 3431−3438.
105. Song, P.-S., and Kurtin, W. E. (1969) *J. Am. Chem. Soc. 91*, 4892−4906.
106. Yamamoto, Y., and Tanaka, J. (1972) *Bull. Chem. Soc. Jpn. 45*, 1362−1366.
107. Eftink, M. R. (1991) *Methods Biochem. Anal. 35*, 127−205.
108. Albinsson, B., and Norden, B. (1992) *J. Phys. Chem. 96*, 6204−6212.
109. Ruggiero, A. J., Todd, D. C., and Fleming, G. R. (1990) *J. Am. Chem. Soc. 112*, 1003−1014.
110. Bismuto, E., Sirangelo, I., and Irace, G. (1993) *Biochim. Biophys. Acta 1146*, 213−218.
111. Woody, R. W., and Dunker, A. K. (1996) in *Circular Dichroism and the Conformational Analysis of Biomolecules* (Fasman, G. D., Ed.) pp 109−157, Plenum Press, New York.
112. Chattopadhyay, A. (1992) in *Biomembrane Structure and Function: The State of the Art* (Gaber, B. P., and Easwaran, K. R. K., Eds.) pp 153−163, Adenine Press, Schenectady, NY.
113. London, E. (1994) *Biophys. J. 67*, 1368−1369.
114. Ladokhin, A. S., and Holloway, P. W. (1995) *Biophys. J. 69*, 506−517.
115. Meers, P. (1990) *Biochemistry 29*, 3325−3330.
116. Chattopadhyay, A., and McNamee, M. G. (1991) *Biochemistry 30*, 7159−7164.
117. Schiffer, M., Chang, C.-H., and Stevens, F. J. (1992) *Protein Eng. 5*, 213−214.
118. White, S. H., and Wimley, W. C. (1994) *Curr. Opin. Struct. Biol. 4*, 79−86.
119. Reithmeier, R. A. F. (1995) *Curr. Opin. Struct Biol. 5*, 491−500.
120. Matsuzaki, K., Murase, O., Tokuda, H., Funakoshi, S., Fujii, N., and Miyajima, K. (1994) *Biochemistry 33*, 3342−3349.
121. De Kruijff, B. (1994) *FEBS Lett. 346*, 78−82.
122. Resh, M. D. (1994) *Cell 76*, 411−413.
123. Leenhouts, J. M., van den Wijngaard, P. W. J., de Kroon, A. I. P. M., and De Kruijff, B. (1995) *FEBS Lett. 370*, 189−192.
124. Garner, J., and Crooke, E. (1996) *EMBO J. 15,*, 2313−2321.
125. Malhotra, R., Taylor, N. R., and Bird, M. I. (1996) *Biochem. J. 314*, 297−303.
126. Mosior, M., Golini, E. S., and Epand, R. M. (1996) *Proc. Natl. Acad. Sci. U.S.A. 93*, 1907−1912.
127. Gennis, R. B. (1989) in *Biomembranes: Molecular Structure and Function*, pp 155−156, Springer-Verlag, New York.
128. Kim, J., Mosior, M., Chung, L. A., Wu, H., and McLaughlin, S. (1991) *Biophys. J. 60*, 135−148.
129. Lentz, B. R. (1995) *Mol. Membr. Biol. 12*, 65−67.
130. Lakowicz, J. R., and Cherek, H. (1980) *J. Biol. Chem. 255*, 831−834.
131. Kirby, E. P., and Steiner, R. F. (1970) *J. Phys. Chem. 74*, 4480−4490.
132. Quay, S. C., and Tronson, L. P. (1983) *Biochemistry 22*, 700−707.
133. Dougherty, D. A. (1996) *Science 271*, 163−167.
134. Mecozzi, S., West, A. P., and Dougherty, D. A. (1996) *Proc. Natl. Acad. Sci. U.S.A. 93*, 10566−10571.
135. Feix, J. B., Popp, C. A., Venkataramu, S. D., Beth, A. H., Park, J. H., and Hyde, J. S. (1984) *Biochemistry 23*, 2293−2299.
136. Dalton, L. A., McIntyre, J. O., and Fleischer, S. (1987) *Biochemistry 26*, 2117−2130.
137. Sanson, A., Ptak, M., Rigaud, J. L., and Gary-Bobo, C. M. (1976) *Chem. Phys. Lipids 17*, 435−444.
138. Blatt, E., Chatelier, R. C., and Sawyer, W. H. (1984) *Photochem. Photobiol. 39*, 477−483.
139. Thulborn, K. R., and Sawyer, W. H. (1978) *Biochim. Biophys. Acta 511*, 125−140.
140. Klausner, R. D., Bhalla, D. K., Dragsten, P., Hoover, R. L., and Karnovsky, M.J. (1980) *Proc. Natl. Acad. Sci. U.S.A. 77*, 437−441.
141. Pjura, W. J., Kleinfeld, A. M., Klausner, R. D., and Karnovsky, M. J. (1982) *Biophys. J. 37*, 69−71.
142. Granick, S. (1991) *Science 253*, 1374−1379.
143. Ho, C., Slater, S. J., and Stubbs, C. D. (1995) *Biochemistry 34*, 6188−6195.
144. Selsted, M. E., Novotny, M. J., Morris, W. L., Tang, Y.-Q., Smith, W., and Cullor, J. S. (1992) *J. Biol. Chem. 267*, 4292−4295.
145. Dempsey, C. E., and Butler, G. S. (1992) *Biochemistry 31*, 11973−11977.
146. Beschiaschvili, G., and Baeuerle, H.-D. (1991) *Biochim. Biophys. Acta 1068*, 195−200.